International Journal of Greenhouse Gas Control 28 (2014) 147–155

Contents lists available at ScienceDirect

International Journal of Greenhouse Gas Control

journal homepage: www.elsevier.com/locate/ijggc

The effects of SO_2 contamination, brine salinity, pressure, and temperature on dynamic contact angles and interfacial tension of supercritical CO_2/brine/quartz systems

Soheil Saraji*, Mohammad Piri, Lamia Goual

Department of Chemical and Petroleum Engineering, University of Wyoming, 1000 E. University Avenue, Laramie, WY 82071-2000, USA

ARTICLE INFO

Article history:
Received 30 September 2013
Received in revised form 13 June 2014
Accepted 16 June 2014

Keywords:
Interfacial tension
Contact angle
Supercritical CO_2
SO_2
Brine salinity
Quartz

ABSTRACT

The successful implementation of geologic CO_2 sequestration schemes in deep saline aquifers requires storage sites with minimum risk of CO_2 leakage through the caprock and maximum storage capacity in the reservoir rock. Some of the essential parameters that affect the effectiveness of a storage scheme are the density of CO_2, the interfacial tension between CO_2-rich and aqueous phases, and the wettability of reservoir rock and caprock in contact with these fluids at reservoir conditions (Tokunaga and Wan, 2013). In this study, densities, interfacial tensions, and dynamic contact angles of CO_2/brine/quartz systems at high temperatures and pressures were simultaneously measured using the Axisymmetric Drop Shape Analysis with no-Apex (ADSA-NA) method. Measurements were performed at pressures (2000–4000 psig), temperatures (50–100 °C), and brine salinities (0.2–5 M) relevant to carbon sequestration in deep saline aquifers. These experimental conditions had not been investigated in the past. Additionally, the effect of SO_2 as a co-contaminant (0–6 wt%) was investigated on these parameters for the first time. Contact angle hysteresis was also examined and the possible implications of the results on different CO_2 trapping mechanisms were discussed.

1. Introduction

The growing demand for energy and the absence of reliable alternatives to fossil fuels are causing an increase in carbon dioxide (CO_2) production as a by-product of energy generation. In order to avoid the adverse effects of carbon emissions on the climate, the current viable solution is to reduce CO_2 emissions by improving the energy efficiency and implement effective carbon capture, utilization, and storage schemes. CO_2 has been injected into petroleum reservoirs for enhanced oil recovery (EOR) since the 1970s (Tomski et al., 2013). Although this scheme has been successful, limited amounts of carbon are currently stored with this approach (Tomski et al., 2013). The increase in the amount of CO_2 that will have to be stored due to prospectively tighter regulations on carbon emissions mandates finding new storage sites. Saline aquifers are promising future sinks of carbon dioxide with potentially high storage capacities. These sinks have been under investigation since the 1990s and there are several successful demonstrations and full-field projects currently active for storage of carbon dioxide in deep saline aquifers across the world (Michael et al., 2010).

Fig. 1 shows the most likely ranges of pressure and temperature at which saline aquifers are found underground. This graph is created considering the earth's surface temperature ranging from 15 to 25 °C, the geothermal gradient between 20 and 30 °C/km, and hydrostatic pressure gradient of about 1500 psi/km. Although there are possible cases of cold reservoirs, for example in the Arctic (Bachu, 2003), or extremely hot reservoirs (Broseta et al., 2012), it is expected that this range is valid for most of the saline aquifers. The phase diagram of carbon dioxide is also superimposed on the same graph, demonstrating that CO_2 is most likely to be in supercritical state in underground aquifers (shaded area in Fig. 1). For the purpose of carbon sequestration, it is desirable to find an aquifer having a pressure and temperature where CO_2 has the highest density so that a maximum mass of carbon dioxide can be stored per unit volume. For pressures higher than 4000 psig (or reservoirs deeper than about 3 km), the density change of CO_2 phase becomes minimal and the cost of compression and injection of CO_2 becomes uneconomical (Bachu, 2003). Also, in agreement with the above argument, the reported CO_2 injection depths for 16 active carbon dioxide storage operations in saline aquifers are between 0.7 and 3 km (Michael et al., 2010). Therefore, we selected pressure and

* Corresponding author. Tel.: +1 3077666601.
E-mail address: ssaraji@uwyo.edu (S. Saraji).

http://dx.doi.org/10.1016/j.ijggc.2014.06.024
1750-5836/

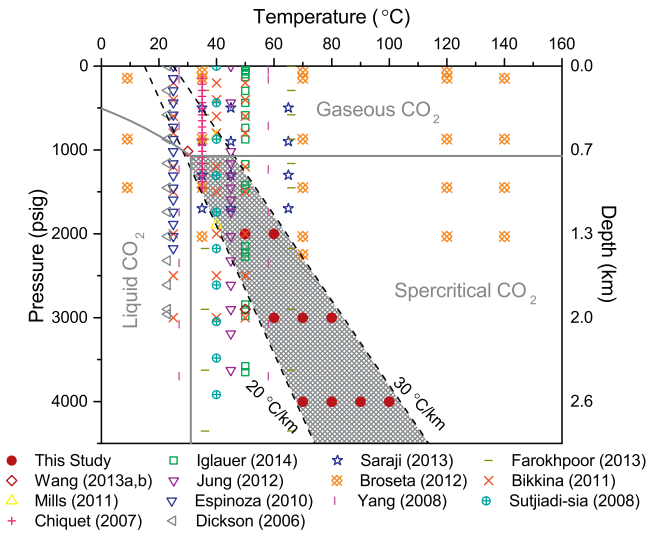

Fig. 1. Experimental pressure and temperature conditions used in this study and in the literature (Broseta et al., 2012; Chiquet et al., 2007; Espinoza and Santamarina, 2010; Farokhpoor, 2013; Jung and Wan, 2012; Wang et al., 2013a, 2013b; Saraji et al., 2013; Bikkina, 2011; Iglauer et al., 2014; Mills et al., 2011; Yang et al., 2008; Dickson et al., 2006; Sutjiadi-Sia et al., 2008). (For interpretation of the references to color in this figure legend, the reader is referred to the web version of this article.)

temperature ranges that were not explored in the past and can be considered more practical for carbon sequestration in deep saline aquifers (filled red circle symbols in Fig. 1).

The salinity of the sedimentary basins that have been used for CO_2 storage varies considerably from 7000 ppm to the maximum salt solubility in water which is about 360,000 ppm (Michael et al., 2010). However, in the United States, the EPA regulations do not permit any CO_2 injection in aquifers with total dissolved solids (TDS) of less than 10,000 ppm (Wilson et al., 2003). Brine salinity is an important parameter that affects the solubility of CO_2, interfacial tension (IFT) between the fluids, wettability of the reservoir rock and caprock, and hence the storage capacity and security of carbon storage in aquifers (Tokunaga and Wan, 2013). The effect of brine salinity on wettability or contact angle (CA) of quartz and glass surfaces in CO_2/brine systems have been recently studied by different research groups (Broseta et al., 2012; Chiquet et al., 2007; Espinoza and Santamarina, 2010; Farokhpoor, 2013; Jung and Wan, 2012; Wang et al., 2013a, 2013b; Mccaughan et al., 2013; Iglauer et al., 2012; Tenney and Cygan, 2014). While some studies did not observe any significant effect of brine salinity on wettability of the substrate (Espinoza and Santamarina, 2010; Wang et al., 2013a, 2013b; Mccaughan et al., 2013; Iglauer et al., 2012; Tenney and Cygan, 2014), others reported a clear decrease in water-wetness of quartz surfaces with an increase in the brine salinity (Broseta et al., 2012; Farokhpoor, 2013; Jung and Wan, 2012; Chiquet et al., 2007). In this study, a broad range of brine salinity (0.2–5 M NaCl), compatible with EPA regulations and currently active CO_2 sequestration projects was investigated.

A report by Miller and Van Atten (2004) listed the annual emissions of about 700 power plants across North America. They have reported 2400 million tons of CO_2 emission into the atmosphere per year from these power plants. Other gases such as Sulfur Dioxide or SO_2 (11.5 million tons per year) and nitrogen oxides or NO_x (4.5 million tons per year) are also present in the emission stream. These gases (co-contaminants) can be co-injected with CO_2 for geological storage, and thereby avoiding extra cost of the separation process. However, there are very limited experimental data on the impact of these chemical species on the geological storage of CO_2 and its security. Furthermore, the wettability state of reservoir minerals and caprock in the presence of, for instance, SO_2 as a co-contaminant has not been studied in the past. There are, currently, very few experimental data exist on the interfacial tension and contact angle of $H_2S + CO_2$ mixture/brine/rock systems at reservoir conditions. Shah et al. (2008) measured the interfacial tension between pure H_2S and 30 mol% $H_2S + CO_2$ mixture in contact with water. They reported a considerable reduction in IFT with increase in H_2S concentration. Broseta et al. (2012) compared the contact angles of CO_2/brine and H_2S/brine on mica and quartz surfaces and did not observe any significant difference between the contact angles of these two fluid systems. For the first time, the effect of SO_2 as a co-contaminant in supercritical CO_2(sc-CO_2) on IFT and dynamic contact angles of a representative system for geological storage of carbon dioxide were examined in this study.

An experimental setup (Saraji et al., 2013) was used to simultaneously measure densities, interfacial tensions, and dynamic contact angles of CO_2/brine/quartz systems. Measurements were performed at pressures (2000–4000 psig), temperatures (50–100 °C), and brine salinities (0.2–5 M) relevant to carbon sequestration in deep saline aquifers (Fig. 1). The effect of SO_2 as a co-contaminant in supercritical CO_2 (0–6 wt%) on fluid densities, interfacial tensions and dynamic contact angles was also investigated. The contact angle hysteresis was calculated and its correlation with pressure, temperature, brine salinity, and SO_2 content was examined.

In this paper, we first present a brief description of the experimental setup and measurement procedures. The effects of temperature, pressure, brine salinity, and SO_2 concentration on the above-mentioned properties are examined next. Lastly, possible implications of the observed trends on the geological sequestration of carbon dioxide are discussed.

2. Materials and methods

2.1. Materials

Materials include: isopropyl alcohol (HPLC grade, Sigma-Aldrich), sulfuric acid (95–98%, ACS grade, Sigma-Aldrich), SuperSmooth™ quartz slides (SPI supplies) with surface roughness smaller than 0.5 nm, NOCROMIX (Godax Laboratories, Inc.), nitrogen (instrumental grade, Praxair, Inc.), CO_2 (instrumental grade, Praxair, Inc.), and anhydrous SO_2 (instrumental grade, Praxair, Inc.). The CO_2 gas cylinders were equipped with a Syphon tube for liquid withdrawal and the distilled water was freshly obtained from an in-house all-glass water distiller.

2.2. Experimental setup

An IFT/CA apparatus (Saraji et al., 2013) was utilized to perform measurements at high pressures (up to 4000 psig) and temperatures (up to 100 °C). The experimental setup, shown in Fig. 2, can handle highly corrosive fluids since all wetted parts are made out of Hastelloy C-276, polyether ether ketone (PEEK), Sapphire glass, and AFLAS O-rings. In this system, a fluid equilibration module enabled the pre-equilibration between partially miscible phases before the measurements. A temperature-controlling module provided accurate and stable temperatures inside the measurement cell (±0.05 °C). A dual-cylinder pulse-free Quizix pump allowed transfer of the equilibrated phases from the equilibration module into the measurement cell at constant pressure. It also provided low and stable flow rates for injection/retraction of CO_2 bubble during the measurements. An Anton Paar DMA HPM density meter, made out of Hastelloy C-276, was used to measure the densities of equilibrated fluids at elevated pressures and temperatures. Before IFT and CA measurements for CO_2/brine/quartz system, the experimental procedures and measurement techniques were carefully validated

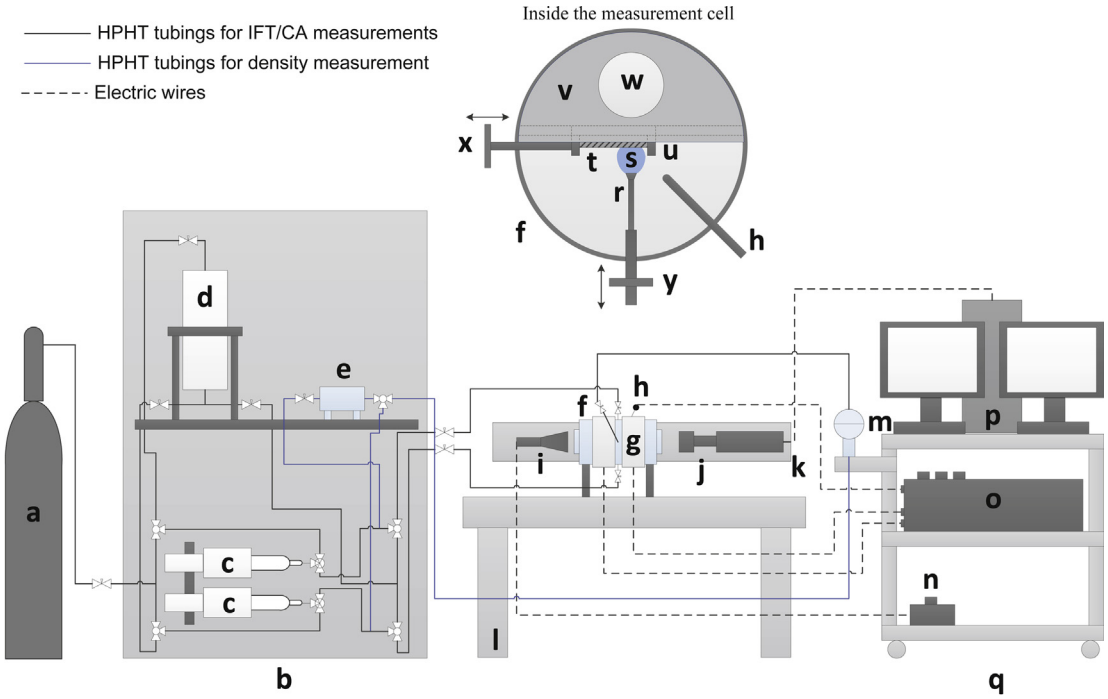

Fig. 2. Schematic of the experimental setup used in this study; (a) CO_2 cylinder, (b) mechanical convection oven, (c) dual-cylinder Quizix pump, (d) equilibration cell, (e) density meter, (f) measurement cell, (g) heating jackets, (h) RTD, (i) light source, (j) apochromatically-corrected lenses and CCD camera, (k) adjustable stand, (l) anti-vibration table, (m) Rosemount pressure sensor, (n) current source, (o) temperature control system, (p) data acquisition computer, (q) shelf cart, (r) IFT/CA needle, (s) fluid bubble, (t) solid substrate, (u) movable tray, (v) crystal holder, (w) fluid level observation opening, (x) horizontal drive shaft, and (y) vertical drive shaft.

with the experimental data available in the literature. The details of the experimental setup and also the validation procedure can be found in Saraji et al. (2013).

In this study, captive bubble configuration was used for IFT/CA measurements. Images of bubbles were captured through a microscope with fully apochromatically corrected lenses attached to a high-resolution digital camera with a standard resolution of 2048×1536 (3 megapixels). The images were analyzed using a well-established technique, i.e. axisymmetric drop shape analysis with no apex (ADSA-NA) (Kalantarian et al., 2009), to simultaneously calculate the interfacial tension and dynamic contact angles of CO_2 bubbles in brine. In this technique, the profile of a bubble captured in an image is extracted by an edge detection method. The program then fits a theoretical Laplacian curve to the experimental profile extracted from the image with the assumption of an axisymmetric bubble shape. Afterwards, the value of IFT is determined from the best match between these two profiles. It then uses the final optimum theoretical profile to find the contact angle at the solid surface level. By convention, the contact angle is measured through the denser fluid (i.e. aqueous phase). It has been shown that contact angles can be measured with an accuracy of 0.2° with this method (Kalantarian et al., 2009). Further details about this technique can be found elsewhere (Kalantarian et al., 2009).

2.3. Substrate preparation

The quartz substrates were prepared with a specific procedure to ensure clean surfaces (i.e. strongly water-wet). A 10% NOCROMIX in sulfuric acid solution was used as the cleaning agent and the substrates were then boiled in distilled water to ensure acid-free hydroxylated surfaces. The substrates were handled from their edges with clean tweezers to avoid surface contamination throughout the preparation stage. A few minutes before each test, the substrates were removed from the distilled water bath and dried by absorbing the bulk water remaining on them with a filter paper (at the edges) and then blow-drying with ultrahigh-purity (UHP) nitrogen. Afterwards, the quartz substrate was mounted on a PEEK crystal holder and then installed inside the measurement cell.

2.4. Experimental procedure

The fluids were pre-equilibrated before measurements in the equilibration cell for about 10–12 h to produce equilibrated CO_2-rich and aqueous phases at the desired pressure (P) and temperature (T). Prior to IFT/CA measurements, the densities of equilibrated phases were measured at the same P and T. The measurement cell was pressurized with CO_2 and temperature was adjusted to the desired experimental conditions. The cell was then filled with the aqueous phase at constant pressure until the solid substrate (quartz) was fully immersed in brine. The fluids and the solid remained inside the measurement cell for about 2 h before the IFT and CA measurements were performed. A pedestal-shaped needle with 1.37 mm outer diameter at the tip was selected based on Bond number calculations for a representative system. It was then used for all the measurements in this study. The needle was utilized to form CO_2 bubbles beneath the quartz substrate, while the needle tip was kept at 3–4 mm from the quartz surface. With this configuration, it was possible to conduct measurements on different areas of the same quartz surface by moving the substrate horizontally. Each substrate was used only once to avoid any possible contaminations.

In order to facilitate the detection of the substrate surface during contact angle measurements, the camera was tilted 1–2° upward with respect to the horizontal line. This approach allowed the mirror image of the bubble on the substrate to be captured in the digital image. A simple mathematical criterion was used to determine the cut off pixel (substrate surface) in all of the images. We first considered a few hundred pixels on the bubble surface (BS) near the contact line together with their mirror image (MI). The substrate surface was defined as the average midpoint between vertically

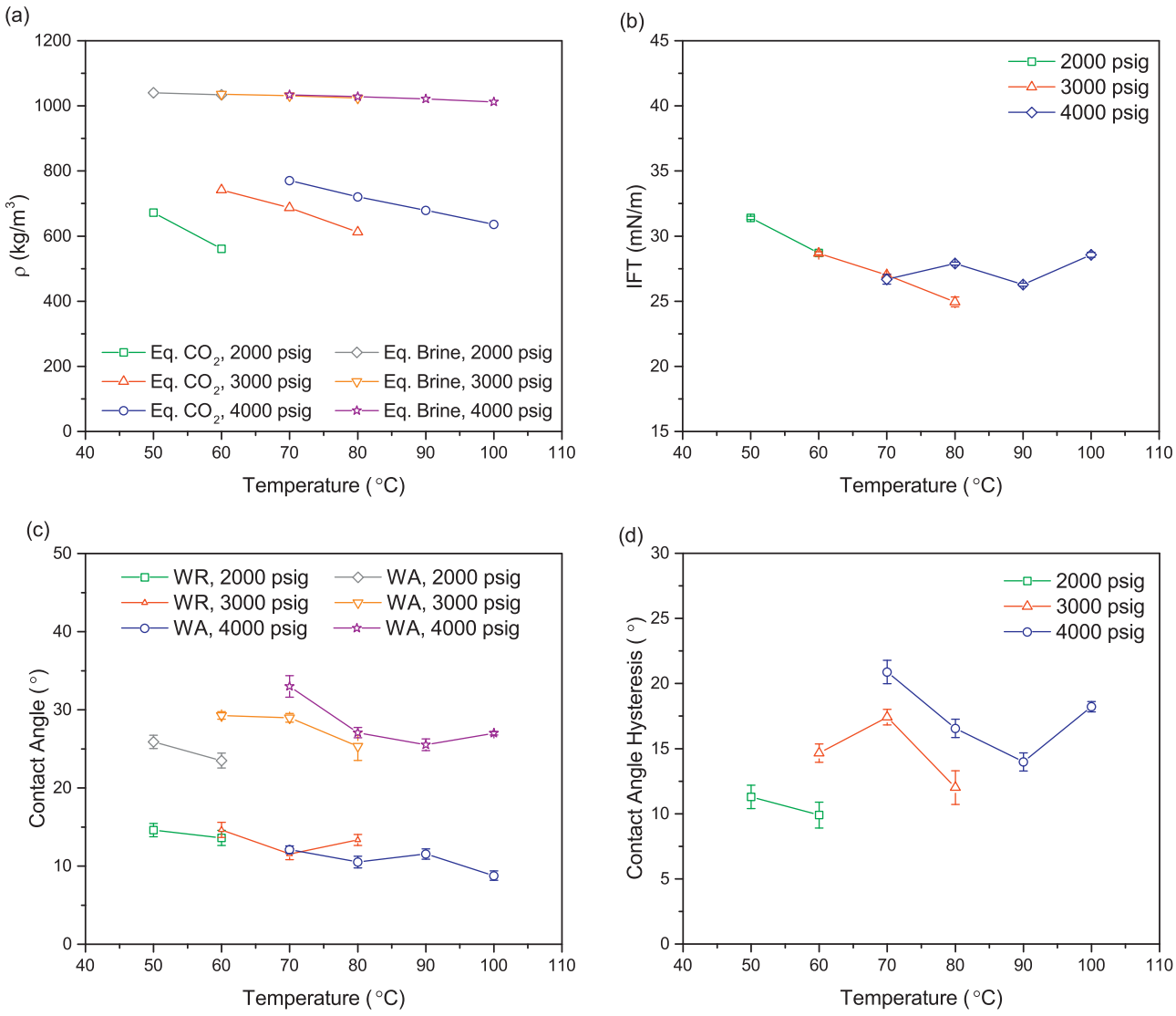

Fig. 3. Effects of pressure and temperature on (a) density, (b) interfacial tension, (c) dynamic contact angles (WR: water receding, WA: water advancing), and (d) contact angle hysteresis ($\Delta\theta$) of CO_2/brine/quartz system.

aligned BS and MI pixels. This algorithm was applied on two sides of the bubble and the two cut off values were utilized for contact angle measurement. Images of the CO_2 bubble were taken repeatedly while the bubble was growing (water receding contact angle) or shrinking (water advancing contact angle) at intervals of 5 s. The ADSA-NA software was used to calculate both IFT and CA from the same images of the captive bubbles. The primary input parameters required for the calculations were the density difference between the fluid phases, acceleration of gravity, image scales, and the location of the solid surface.

3. Results and discussion

In order to investigate the effects of pressure (2000–4000 psig), temperature (50–100 °C), brine salinity (0.2–5 M), and SO_2 concentration in CO_2 (0–6 wt%) on IFT and CA of sc-CO_2/brine/quartz, 17 separate tests were performed. Table 1 lists the densities of equilibrated phases, interfacial tensions between fluids, as well as water advancing and receding contact angles measured under above-mentioned conditions. All the data presented in this table are the average of 3–5 measurements.

3.1. Natural wettability of quartz surface

The effect of surface contamination on contact angle measurements in CO_2/brine/quartz systems was first addressed in a communication between Bikkina (2011, 2012) and Mahadevan (2012). Later, Saraji et al. (2013) pointed out the possibility of contamination as a major source of discrepancy in the reported contact angles for such systems. They proposed an extensive substrate cleaning procedure, storage in distilled water before use, and drying the surface with ultrahigh-purity nitrogen as necessary steps to avoid surface contamination. Most recently, Iglauer et al. (2014) investigated the effect of the cleaning procedure on contact angle of CO_2/brine on quartz/glass surfaces and concluded that inappropriate cleaning methods could result in artificially high contact angles. They reported relatively low contact angles (0–30°) for clean surfaces, which is consistent with the values reported by Saraji et al. (2013). However, using oxidizing solutions such as Piranha (Iglauer et al., 2014) and NOCROMIX in sulfuric acid solution (Saraji et al., 2013) may cause hydroxylation of the quartz surface and hence change its wettability. Therefore, it is important to understand the natural wettability of quartz surface at conditions relevant to carbon sequestration before coming into contact with CO_2 phase.

Table 1
Density, interfacial tension, and water advancing and receding contact angles of CO_2/brine/quartz systems measured in this study. (The reported errors in this table are the standard deviation of the mean value.).

Test	P (psig)	T (°C)	Ionic strength (M)	SO_2 (wt%)	ρ_{CO_2} (kg/m^3)	ρ_{Brine} (kg/m^3)	$\Delta\rho$ (kg/m^3)	IFT (mN/m)	θ_{WR} (°)	θ_{WA} (°)	$\Delta\theta$ (°)
1	2000	50	1	0	672	1040	369	31.4 ± 0.1	14.6 ± 0.9	25.9 ± 0.9	11.3 ± 0.9
2	2000	60	1	0	561	1034	473	28.7 ± 0.2	13.6 ± 1.0	23.5 ± 1.0	9.9 ± 1.0
3	3000	60	1	0	742	1036	294	28.7 ± 0.1	14.6 ± 1.0	29.3 ± 0.5	14.7 ± 0.7
4	3000	70	1	0	687	1031	345	27.0 ± 0.1	11.6 ± 0.7	29.0 ± 0.6	17.4 ± 0.6
5	3000	80	1	0	612	1024	412	25.0 ± 0.4	13.3 ± 0.7	25.4 ± 1.8	12.0 ± 1.3
6	4000	70	1	0	771	1034	264	26.7 ± 0.4	12.1 ± 0.5	33.0 ± 1.4	20.9 ± 0.9
7	4000	80	1	0	721	1028	307	27.9 ± 0.1	10.5 ± 0.8	27.1 ± 0.7	16.6 ± 0.7
8	4000	90	1	0	679	1021	342	26.3 ± 0.1	11.5 ± 0.7	25.5 ± 0.8	14.0 ± 0.7
9	4000	100	1	0	636	1012	377	28.6 ± 0.2	8.8 ± 0.6	27.0 ± 0.2	18.2 ± 0.4
10	3000	60	0.2	0	740	1010	270	26.0 ± 0.3	10.0 ± 0.2	20.5 ± 0.9	10.5 ± 0.5
11	3000	70	0.2	0	674	1003	329	23.9 ± 0.2	9.8 ± 0.7	16.5 ± 1.0	6.7 ± 0.8
12	3000	80	0.2	0	614	996	382	23.6 ± 0.2	11.0 ± 0.7	17.0 ± 1.9	6.0 ± 1.3
13	3000	60	5	0	739	1166	427	39.2 ± 0.2	17.3 ± 0.9	35.7 ± 0.7	18.4 ± 0.8
14	3000	70	5	0	674	1162	488	39.2 ± 0.7	19.8 ± 1.2	44.1 ± 1.5	24.2 ± 1.4
15	3000	80	5	0	613	1147	534	38.3 ± 0.8	20.0 ± 1.4	42.2 ± 2.1	22.2 ± 1.7
16	3000	60	1	1	739	1022	283	27.0 ± 0.4	14.0 ± 0.1	27.0 ± 0.2	13.0 ± 0.2
17	3000	60	1	6	778	1023	245	18.4 ± 0.7	12.9 ± 1.0	27.6 ± 2.5	14.7 ± 1.7

The previous studies on the surface chemistry of silica suggest that the wettability of silica surface is largely determined by the arrangement and distribution of surface groups such as silanol (Si—OH) and siloxane (Si—O—Si) (Iler, 1979; Vansant, 1995). For instance, a recent molecular dynamics simulation study reported approximately 10° increase in water-CO_2 contact angle by increasing the silanol surface density on quartz from 1.7 to 4.5 (OH/nm^2) (Mccaughan et al., 2013). The reason for this behavior is the preferential adsorption of water molecules on hydrophilic silanols rather than hydrophobic siloxanes (Iler, 1979). Moreover, thermal treatment of silica at very high temperatures (>400 °C) was shown to cause dehydroxylation of its surface, meaning conversion of silanols to siloxanes (Vansant, 1995). For example, Horn et al. (1989) reported a relatively high contact angle (i.e. 45°) on freshly prepared high-purity silica surface by the melting method (the melting point of silica is around 1600 °C). In contrast, soaking silica in water is believed to result in rehydroxylation of silica surface (Vansant, 1995). This process is exceedingly slow at 25 °C, and it is recommended to heat silica in water at 95 °C for several hours to rehydroxylate the surface (Iler, 1979). This is also in accord with the reported water contact angles on hydrophilic quartz/glass surfaces (<10°) measured by different methods such as Wilhelmy plate (Mennella and Morrow, 1995), capillary rise (Siebold et al., 2000), and sessile drop (Sumner et al., 2004).

Therefore, the surface of quartz minerals in contact with aquifer at subsurface conditions, in extended geological time scales, is expected to be hydroxylated. Although one can argue that the quartz grains in reservoir rocks are partly covered by omnipresent clays, the clean pure hydroxylated quartz surface (strongly water-wet) provides a practical baseline for fundamental research on fluid-mineral interactions during geological sequestration of carbon dioxide.

3.2. Effects of pressure and temperature

The pressure and temperature ranges used in this study are 2000–4000 psig and 50–100 °C, respectively, as shown in Fig. 1. Experiments were performed at nine different conditions, all with a brine salinity of 1 M. Because brine is largely incompressible in the pressure and temperature range of these experiments, its density was not affected by pressure change; although it slightly decreased when temperature was increased (Fig. 3a). On the other hand, supercritical carbon dioxide (sc-CO_2) is a compressible fluid and its density increased with increasing pressure and decreased with increasing temperature (Fig. 3a). The interfacial tension between equilibrated CO_2-rich and aqueous phases at various temperatures

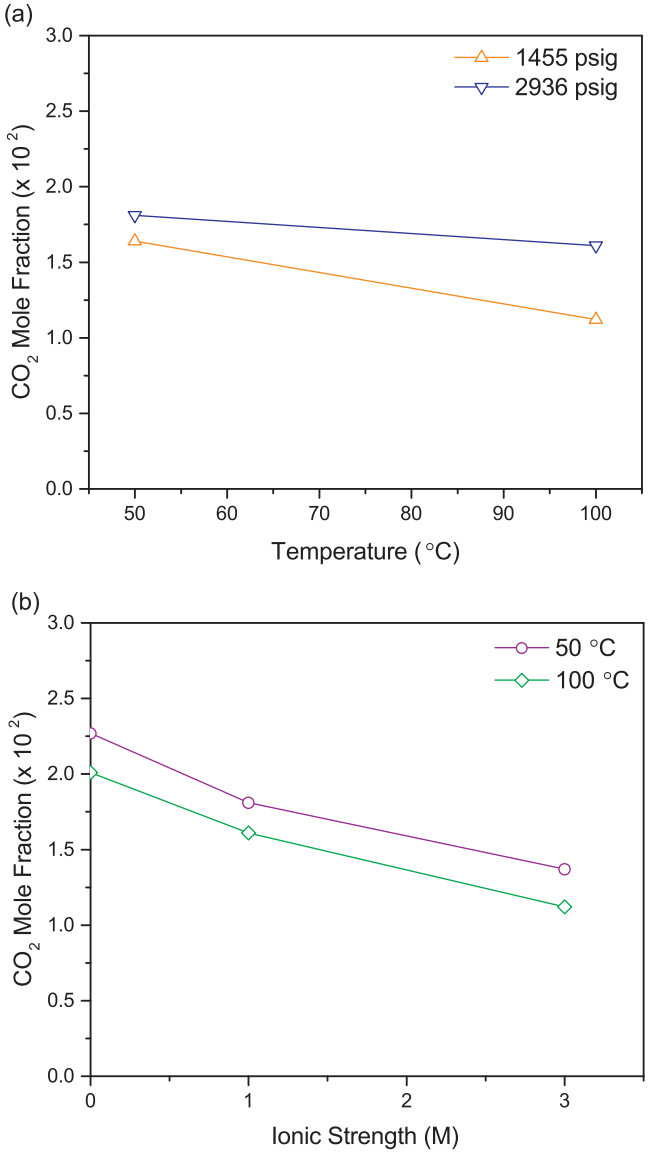

Fig. 4. Variations in CO_2 solubility in brine with (a) pressure and temperature (1 M brine), and (b) brine salinity (at 3000 psig) (data from Koschel et al. (2006)).

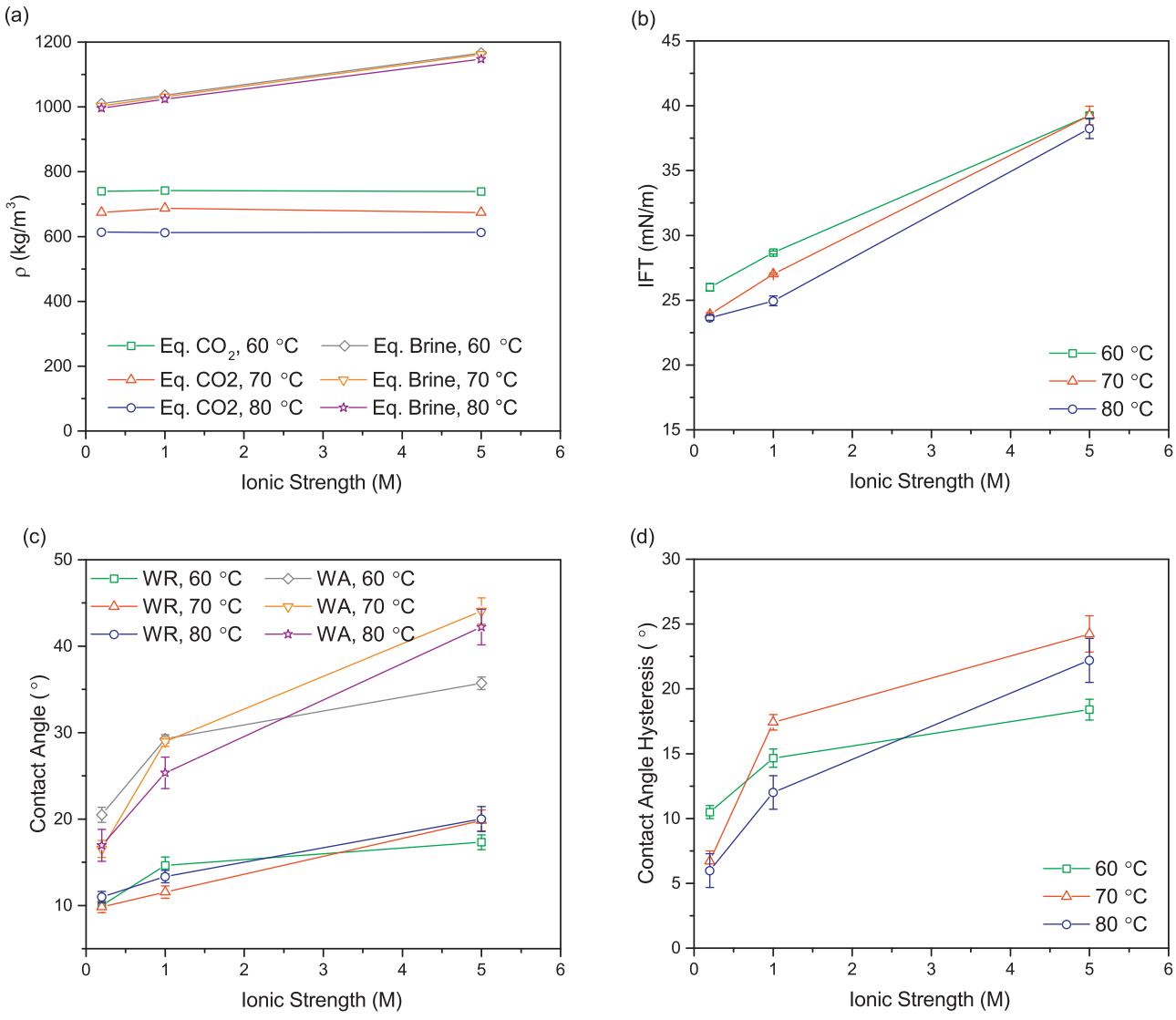

Fig. 5. Effects of brine salinity on (a) density, (b) interfacial tension, (c) dynamic contact angles (WR: water receding, WA: water advancing) and (d) contact angle hysteresis ($\Delta\theta$) of CO_2/brine/quartz system. (All the measurements were performed at 3000 psig.)

and pressures are plotted in Fig. 3b. As shown in this figure, variations in pressure did not have a significant effect on the IFT, but an increase in temperature slightly reduced the IFT values. Fig. 4a shows the experimental CO_2 solubility data in 1 M brine and its variations with P and T reported in Koschel et al. (2006). The relative insensitivity of IFT to P and T in the supercritical region of CO_2 may stem from the fact that the solubility of CO_2 in brine (1 M) does not drastically change in the P and T ranges studied here. Similar to the IFT data, the dynamic contact angles also did not change significantly with P and T (Fig. 3c). There was only a slight increase in the contact angles and contact angle hysteresis ($\Delta\theta$) by the increase in pressure (the last column of Table 1 and Fig. 3d). However, due to the lack of enough temperature overlap in the presented data, a general trend cannot be deducted.

3.3. Effect of brine salinity

In a recent publication by Michael et al. (2010), the authors summarized the operational conditions for 16 active sequestration sites worldwide with brine salinities ranging from 7000 to 340,000 ppm. Therefore, three different salinities were chosen for our studies that are in the range of 0.2–5 M NaCl (~11,500–300,000 ppm) to cover the spectrum of brine salinities observed in underground aquifers. All the measurements in this section were performed at 3000 psig.

The densities of CO_2-rich and aqueous phases at various NaCl concentrations are plotted in Fig. 5a. As expected, the density of CO_2 was insensitive to the changes in salt concentration, however brines with the higher ionic strength had larger densities. Fig. 5b depicts the variations of IFT with the ionic strength. There was a significant increase in IFT by an increase in the ionic strength. For example, IFT between equilibrated sc-CO_2 and brine at 3000 psig and 60 °C increased from 26 to 39 mN/m by changing the ionic strength from 0.2 to 5 M. This behavior is partly due to the decrease in CO_2 solubility in brine at higher salinities, as shown in Fig. 4b, and partly because of hydration of ions that leads to an ion-free layer at the water interface (Bachu and Bennion, 2009).

Fig. 5c depicts the water receding and advancing contact angles of the CO_2/brine/quartz system at various brine salinities. There was a consistent increase in both dynamic contact angles with the increase in ionic strength. The observed trend is consistent with the reported data in several studies (Broseta et al., 2012; Chiquet et al., 2007; Farokhpoor, 2013; Jung and Wan, 2012). Furthermore,

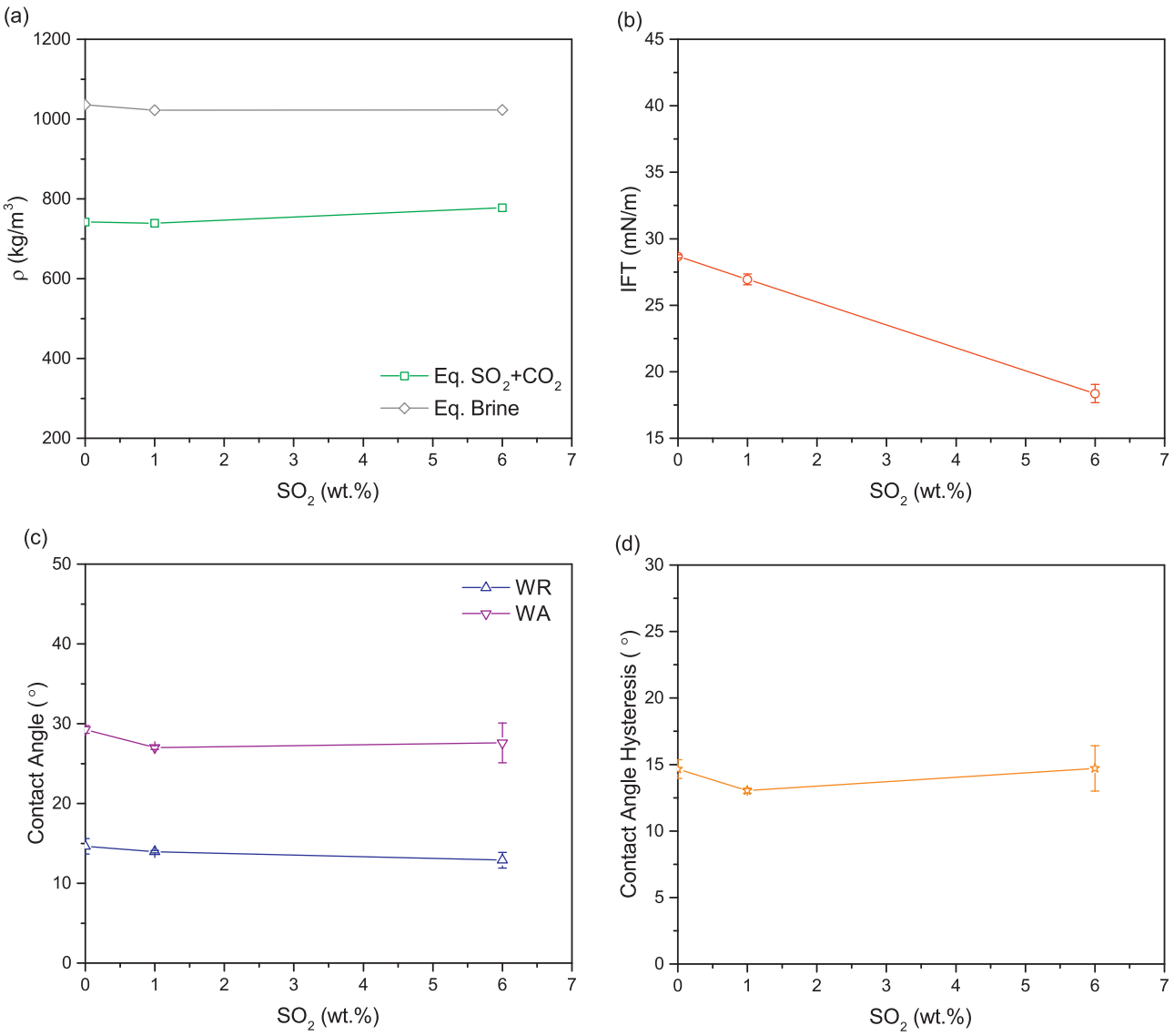

Fig. 6. Effects of SO_2 concentration on (a) density, (b) interfacial tension, (c) dynamic contact angles (WR: water receding, WA: water advancing) and (d) contact angle hysteresis ($\Delta\theta$) of $SO_2 + CO_2$/brine/quartz system. (All the measurements were performed at 3000 psig, 60 °C, and 1 M brine salinity.)

the hysteresis in contact angle was much larger at higher salinities (Fig. 5d). For instance, $\Delta\theta$ increased from 6° to 22° with an increase in the brine ionic strength from 0.2 to 5 M at 80 °C.

3.4. *Effect of SO_2 contaminant*

Based on a report by Miller and Van Atten (2004), the SO_2/CO_2 ratio in the emission stream of power plants varies between 0.02 and 8 wt% with an average of 0.6 wt%. Thus, to cover the reported SO_2 range, two CO_2 mixtures with 1 wt% SO_2 (Test 16 in Table 1) and 6 wt% SO_2 (Test 17 in Table 1) content were considered in this study. The pressure (3000 psig), temperature (60 °C), and brine salinity (1 M) were kept constant for these experiments.

The densities of equilibrated CO_2-rich phase for $SO_2 + CO_2$ mixtures were larger than those of equilibrated CO_2-rich phase in the absence of SO_2 (Fig. 6a). This is because SO_2 has a higher density than CO_2. In spite of this, the densities of aqueous phases were slightly smaller in the presence of SO_2. This results in a decreasing trend of $\Delta\rho$ with increasing SO_2 concentration (Table 1). Fig. 6b shows that the interfacial tension between equilibrated phases decreased linearly with increase in the SO_2 concentration. There was a significant decrease in IFT (i.e. 40%) from 29 mN/m in the case of pure CO_2 to 18 mN/m in the presence of 6 wt% SO_2. A recent study (Tarbuck and Richmond, 2006) on the effect of SO_2 and CO_2 molecules on the gas/water interface was performed by comparing OH stretching intensities at the interfacial water spectrum. This study showed a clear difference between the interactions of these two molecules with water (Tarbuck and Richmond, 2006). The authors observed that a weakly bounded surface complex was formed between SO_2 and interfacial water molecules, which affected the molecular structure at the interface. However, no specific surface-bound species were observed in the case of pure CO_2. The presence of this weakly bounded surface complex between SO_2 and water molecules at the supercritical fluid/liquid interface could be the main contributor for the considerable decrease in IFT values. Similar effects on the IFT of CO_2/brine in the presence of another acid gas (i.e. H_2S) have also been reported (Shah et al., 2008). The IFT between $H_2S + CO_2$ mixtures and brine under conditions comparable to our experiments dropped from 32 mN/m (pure CO_2) to 26 mN/m (30 mol% H_2S) and 7.5 mN/m (pure H_2S).

The dynamic contact angles and hysteresis for $SO_2 + CO_2$/brine/quartz system are shown in Fig. 6c and d. We have not observed any

significant change in water receding/advancing contact angles and CA hysteresis by increasing SO_2 concentration. This is comparable with the work of Broseta et al. (2012) who did not observe any major change in the wettability of quartz when switching from pure CO_2 to pure H_2S.

3.5. Potential implications for CO_2 storage

The main trapping mechanisms of sc-CO_2 in a saline aquifer include: structural/stratigraphic, capillary, solubility, and mineral trappings. The capacity of an aquifer to safely hold CO_2 underground as free gas (structural trapping) depends on the threshold capillary pressure of the caprock (Pc_{th}). Based on the Young–Laplace equation (i.e., $P_c = \frac{2IFT\ \cos(CA)}{r}$, r: characteristic pore radius), Pc_{th} is in turn determined by the interfacial tension between CO_2-rich and aqueous phases and water receding contact angle (CO_2 displacing water) (Chiquet et al., 2007). A higher threshold pressure promotes the safe storage of carbon and increases the storage capacity of the aquifer. Also, the water advancing contact angle affects the amount of CO_2 that can be trapped as the immobile phase during water imbibition in the reservoir (capillary trapping). In water-wet systems, the lower water advancing contact angles translate to larger volumes of trapped CO_2 phase. Another critical parameter of the system is the density of CO_2 in the reservoir. At higher CO_2 densities, greater mass of carbon can be stored per unit volume of the reservoir rock.

Within the P–T range studied here, the interfacial tension and water receding contact angles of CO_2/brine/quartz systems were only slightly affected by changes in P and T. Therefore one can expect no significant effect on the threshold capillary pressure of the caprock and the capacity for free gas storage in a saline aquifer. Moreover, the water advancing contact angle slightly increased with increasing the pressure and mildly decreased with increasing the temperature. Hence, no significant change is expected in the capillary trapping of CO_2 with depth. On the other hand, the density of CO_2 phase is highly sensitive to both P and T and rises with depth (Bachu, 2003). Thus the capacity of an aquifer for holding CO_2 both as free and trapped phases increases with depth to about 3–4 km. For aquifers deeper than 4 km, the density becomes insensitive to P and T and therefore remains fairly constant with depth (Bachu, 2003).

The increase in brine salinity caused a considerable increase in IFT and a slight increase in water receding contact angle. Small changes in contact angle can be ignored compared to large changes in IFT. Consequently, the overall effect of brine salinity is an increase in the threshold capillary pressure of the caprock, hence improved security of CO_2 storage as free gas. Conversely, the water advancing contact angle increased at higher salt concentrations while the density of CO_2 phase remained unaffected. Therefore, at higher salinities the amount of capillary trapped CO_2 is expected to decrease for a given porous medium (at constant P and T). Also, as mentioned earlier, the solubility of CO_2 in brine reduces at higher ionic strengths and hence the capacity of brine to dissolve CO_2 declines (solubility trapping). Therefore, the overall capacity of the aquifer with changes in brine salinity depends on the competition between these three trapping mechanisms.

The presence of SO_2 as a co-contaminant in CO_2-rich phase resulted in a significant decrease in IFT with brine while it did not affect the water receding/advancing contact angles. As a result, we expect Pc_{th} to decrease considerably. Unfortunately, the effect of SO_2 on solubility trapping of CO_2-rich phase in brine is unknown due to the lack of experimental data. Nevertheless, the results presented here suggest co-injection of $SO_2$with carbon dioxide at relatively low concentrations may increase the risk of capillary failure of caprocks by reducing the IFT.

4. Conclusions

Densities, interfacial tensions, and dynamic contact angles of equilibrated CO_2 and brine on quartz surface were measured at pressure and temperature conditions relevant to deep saline aquifers. The results indicated that pressure and temperature variations, within the range studied, did not significantly affect IFT and CA. Also, contact angle hysteresis was only slightly changed by these parameters. On the other hand, an increase in brine salinity resulted in an increase in IFT, CA, and CA hysteresis. Furthermore, the effect of SO_2 as a co-contaminant on densities, IFT, and CA of the system was studied for the first time. While rock wettability was not affected by SO_2, the IFT between $CO_2 + SO_2$ mixture and brine decreased linearly with increase in the amount of SO_2 in the CO_2-rich phase. Therefore, the co-injection of SO_2 at high concentrations in saline aquifers may increase the risk of gas leakage though the caprock.

Acknowledgments

This work was supported by DOE Financial Assistance Agreement DE-FE0004832. The authors also acknowledge the financial support of the School of Energy Resources and the Enhanced Oil Recovery Institute at the University of Wyoming.

References

Tokunaga, T.K., Wan, J., Nov 2013. Capillary pressure and mineral wettability influences on reservoir CO_2 capacity. Rev. Miner. Geochem. 77 (1), 481–503.
Tomski, P., Kuuskraa, V., Moore, M., 2013. US Policy Shift to Carbon Capture, Utilization, and Storage Driven by Carbon Dioxide Enhanced Oil Recovery.
Michael, K., Golab, a., Shulakova, V., Ennis-King, J., Allinson, G., Sharma, S., Aiken, T., Jul 2010. Geological storage of CO_2 in saline aquifers—a review of the experience from existing storage operations. Int. J. Greenh. Gas Control 4 (4), 659–667.
Bachu, S., Jun 2003. Screening and ranking of sedimentary basins for sequestration of CO_2 in geological media in response to climate change. Environ. Geol. 44 (3), 277–289.
Broseta, D., Tonnet, N., Shah, V., Nov 2012. Are rocks still water-wet in the presence of dense CO_2 or H_2S? Geofluids 12 (4), 280–294.
Wilson, E.J., Johnson, T.L., Keith, D.W., Aug 2003. Regulating the ultimate sink: managing the risks of geologic CO_2 storage. Environ. Sci. Technol. 37 (16), 3476–3483.
Chiquet, P., Broseta, D., Thibeau, S., May 2007. Wettability alteration of caprock minerals by carbon dioxide. Geofluids 7 (2), 112–122.
Espinoza, D.N., Santamarina, J.C., Jul 2010. Water–CO_2–mineral systems: interfacial tension, contact angle, and diffusion-implications to CO_2 geological storage. Water Resour. Res. 46 (7), W07537.
Farokhpoor, R., Bjørkvik, B.J.a., Lindeberg, E., Torsæter, O., Jan 2013. Wettability behaviour of CO_2 at storage conditions. Int. J. Greenh. Gas Control 12, 18–25.
Jung, J., Wan, J., 2012. Supercritical CO_2 and ionic strength effects on wettability of silica surfaces: equilibrium contact angle measurements. Energy Fuels 26, 6053–6059.
Wang, S., Tao, Z., Persily, S.M., Clarens, A.F., Oct 2013. CO_2 adhesion on hydrated mineral surfaces. Environ. Sci. Technol. 47 (20), 11858–11865.
Mccaughan, J., Iglauer, S., Bresme, F., 2013. Molecular dynamics simulation of water/CO_2–quartz interfacial properties: application to subsurface gas injection. Energy Proc. 37, 5387–5402.
Iglauer, S., Mathew, M.S., Bresme, F., 2012. Molecular dynamics computations of brine–CO_2 interfacial tensions and brine–CO_2–quartz contact angles and their effects on structural and residual trapping mechanisms in carbon geosequestration. J. Colloid Interface Sci. 386, 405–414.
Wang, S., Edwards, I.M., Clarens, A.F., Jan 2013. Wettability phenomena at the CO_2–brine–mineral interface: implications for geologic carbon sequestration. Environ. Sci. Technol. 47 (1), 234–241.
Tenney, C.M., Cygan, R.T., Feb 2014. Molecular simulation of carbon dioxide, brine, and clay mineral interactions and determination of contact angles. Environ. Sci. Technol. 48 (3), 2035–2042.
Miller, P.J., Van Atten, C., 2004. North American Power Plant Emissions.
Shah, V., Broseta, D., Mouronval, G., Montel, F., Oct 2008. Water/acid gas interfacial tensions and their impact on acid gas geological storage. Int. J. Greenh. Gas Control 2 (4), 594–604.
Saraji, S., Goual, L., Piri, M., Plancher, H., Jun 2013. Wettability of supercritical carbon dioxide/water/quartz systems: simultaneous measurement of contact angle and interfacial tension at reservoir conditions. Langmuir 29 (23), 6856–6866.
Kalantarian, A., David, R., Neumann, A.W., Dec 2009. Methodology for high accuracy contact angle measurement. Langmuir 25 (24), 14146–14154.
Bikkina, P.K., Sep 2011. Contact angle measurements of CO_2–water–quartz/calcite systems in the perspective of carbon sequestration. Int. J. Greenh. Gas Control 5 (5), 1259–1271.

Bikkina, P.K., Mar 2012. Reply to the comments on contact angle measurements of CO_2–water–quartz/calcite systems in the perspective of carbon sequestration. Int. J. Greenh. Gas Control 7, 263–264.
Mahadevan, J., Mar 2012. Comments on the paper titled 'Contact angle measurements of CO_2–water-quartz/calcite systems in the perspective of carbon sequestration': a case of contamination? Int. J. Greenh. Gas Control 7, 261–262.
Iglauer, S., Salamah, A., Sarmadivaleh, M., Liu, K., Phan, C., Mar 2014. Contamination of silica surfaces: impact on water–CO_2–quartz and glass contact angle measurements. Int. J. Greenh. Gas Control 22, 325–328.
Iler, R.K., 1979. The chemistry of silica: solubility, polymerization. In: Colloid and Surface Properties and Biochemistry of Silica, 1st ed. John Wiley & Sons, Inc., New York, pp. 866.
Vansant, E.F., Der Voort, P.V., Vrancken, K.C., 1995. Characterization and Chemical Modification of the Silica Surface, 1st ed. Elsevier B.V., Amsterdam, pp. 556.
Horn, R.G., Smith, D.T., Haller, W., 1989. Surface forces and viscosity of water measured between silica sheets. Chem. Phys. Lett. 162 (4–5).
Mennella, A., Morrow, N.R., 1995. Point-by-point method of determining contact angles from dynamic Wilhelmy plate data for oil/brine/solid systems. J. Colloid Interface Sci. 172 (1), 48–55.
Siebold, A., Nardin, M., Schultz, J., 2000. Effect of dynamic contact angle on capillary rise phenomena. Colloids Surf. A Physicochem. Eng. Asp. 161, 81–87.
Sumner, A.L., Menke, E.J., Dubowski, Y., Newberg, J.T., Penner, R.M., Hemminger, J.C., Wingen, L.M., Brauer, T., Finlayson-pitts, B.J., 2004. The nature of water on surfaces of laboratory systems and implications for heterogeneous chemistry in the troposphere. Phys. Chem. Chem. Phys. 6 (3), 604–613.
Koschel, D., Coxam, J.-Y., Rodier, L., Majer, V., Sep 2006. Enthalpy and solubility data of CO_2 in water and NaCl(aq) at conditions of interest for geological sequestration. Fluid Phase Equilib. 247 (1–2), 107–120.
Bachu, S., Bennion, D.B., 2009. Interfacial tension between CO_2, freshwater, and brine in the range of pressure from (2 to 27) MPa temperature from (20 to 12) °C, and water salinity from (0 to 334 000) mg L^{-1}. J. Chem. Eng. Data 54 (3), 765–775.
Tarbuck, T.L., Richmond, G.L., 2006. Adsorption and reaction of CO_2 and SO_2 at a water surface. J. Am. Chem. Soc. 128 (10), 3256–3267.
Mills, J., Riazi, M., Sohrabi, M., 2011. Wettability of common rock-forming minerals in a CO2–brine system at reservoir conditions. SCA2011-06, pp. 1–12.
Yang, D., Gu, Y., Tontiwachwuthikul, P., 2008. Wettability determination of the reservoir brine-reservoir rock system with dissolution of CO_2 at high pressures and elevated temperatures. Energy Fuels 22 (4), 504–509.
Dickson, J.L., Gupta, G., Horozov, T.S., Binks, B.P., Johnston, K.P., Feb 2006. Wetting phenomena at the CO_2/water/glass interface. Langmuir 22 (5), 2161–2170.
Sutjiadi-Sia, Y., Jaeger, P., Eggers, R., 2008. Interfacial tension of solid materials against dense carbon dioxide. J. Colloid Interface Sci. 320, 268–274.